Structural, Optical and Morphological Characteristics of Laser-Treated Graphene Layers Grown on Silicon Substrates by Spin Coating

Shareef F.S. Al-Tikrity
Athraa N. Taha

Department of Physics, College of Science, Tikrit University, Tikrit, IRAQ

This study examined effect of pulsed laser on graphene deposited on silicon substrates of n- and p-type. XRD pattern reveals a hexagonal structure with a high degree of crystallization and a diffraction peak at 26°. The dominating growth direction of graphene is (002). This result, confirmed the decrease in graphene density after treatment. FESEM images of the samples appear as flakes or wrinkled sheets and nano-sized particles. The removal of many graphene layers was observed in both types, wrinkled flakes appear in smooth layers evenly distributed over the surface. For samples deposited on n-type, the particle size dropped from 78 to 54 nm, and on p-type, it reduced from 98 to 66 nm. FTIR spectra showed vibrational groups including carbon=carbon (C=C) at the absorption peak of 1630 cm, the carbonyl (C=O) groups at 1695.43-1705.07 cm-1. The energy gap decreases after laser treatment. These results are important for optoelectronic devices.

Keywords: Graphene nanostructures; Pulsed laser; Structural properties; Morphology
Received: 12 June 2024; Revised: 20 July 2024; Accepted: 27 July 2024

1. Introduction

Nanotechnology, nanoscience and its applications are still developing very rapidly on a large scale in all fields related to materials science, energy and Sensors, as they have occupied many researchers in many fields. Progress in changing the methodologies used in the manufacture of various nanomaterials to suit the requirements of the electronics market has become an urgent necessity. Furthermore, nanomaterials with different structures, sizes, and compositions can be fabricated in a controlled manner, contributing to the relationship between composition, structure, and performance [1,2]. Nanocomposites have a multi-dimensional structure, such as fullerene in zero-dimension, carbon nanotubes in one dimension, and graphene in two dimensions, offering great promise in a wide range of applications, including electro-catalysis, sensing, bioimaging, and more. One of these promising nanomaterials is graphene [3]. Since its discovery in 2004, graphene consists of a single layer of carbon atoms arranged in a two-dimensional lattice structure [4,5]. It consists of carbon atoms that have sp^2 hybridization, arranged in a pattern resembling a hexagonal or honeycomb structure. The thickness of graphene is comparable to the diameter of a single atom. Moreover, graphene is made entirely of carbon atoms, each of which forms covalent bonds in a flat plane. Van der Waals interactions, which are attractive forces, bind single-layer graphene sheets to one another [6,7]. Because of its remarkable thermal, mechanical, chemical, and optical qualities most notably its high electrical mobility, thermal conductivity, and mechanical strength graphene has drawn a lot of attention recently [8-10]. Despite much study, chemical-free and low-temperature processing of high-quality graphene, remains a major challenge to improve the number of layers and morphology of graphene sheets on the substrate. Because graphite sheets are bound together by a high cohesive van der Waals energy, the primary challenge in producing graphene is overcoming the significant peeling energy of stacked layers in graphite.

Heat treatments necessitate annealing and heating at a high temperature, while chemical treatments rely on a very poisonous material. Furthermore, contamination from those operations causes some structural flaws and impurities to be produced in graphene during the layer reduction process [11-13]. Great efforts have been made to manufacture graphene and use it in laser-assisted flexible electronic devices. The laser-based approach is simple, catalyst-free, environmentally friendly, and the process generates no toxic gases. It can be used to reduce graphene layers or modify graphene films and to manufacture electronic devices. The number of layers and the degree of reduction can also be adjusted by changing the laser parameters, i.e., power, scanning speed, pulse frequency and incident laser beam diameter. Increasing the energy of the emitted photons may break the chemical bonds of functional groups attached to graphene for reduction [14,15]. Recently, the emerging technology of laser processing, which combines nanotechnology with "light," has attracted widespread attention from researchers around the world as an effective approach. It holds tremendous promise for modifying the surface or electronic structure of materials in contrast to conventional heat treatment methods, laser irradiation depends on the photo-thermal effect created by a pulsed laser beam, which results in a high temperature range that is controllably restricted to a

particular area and is followed by quick cooling. The applied laser parameters, such as frequency, pulse width, and laser intensity, can readily be adjusted to change the thermal effect. The site-specific photothermal effect and the short processing time are the key benefits of laser processing, since they enable the rapid production of thinner, more appropriate nanomaterials [16-20].

In this work, the spin coating method was used to deposit graphene on silicon surfaces. After that, the thin layers were treated using a pulsed laser to improve their quality and properties. The results showed that this technique enables the production of high-quality graphene layers, which makes these thin graphene layers with promising potential for use. In future optical and electronic applications.

2. Materials and methods

Graphene films preparation, spin coating method was utilized to prepare the films. A graphene solution was prepared by combining graphene platelet nanopowder (SkySpring nanomaterials, USA), ethanol (96%) and Stearic acid ($C_{18}H_{36}O_2$; HIMEDIA, India), which served as a solute–solvent binder. First, 5 mg of stearic acid was dissolved in 50 ml of ethanol while continuously stirring and heating on a hot plate stirrer. After it dissolved completely, 250 mg of graphene was added to solution and continued stirring and heating for 5 minutes until a clear and uniform solution is obtained. This final solution was used as a coating source after cooling to room temperature. Graphene thin films were deposited on n-type and p-type silicon substrates by spin coating at room temperature. The coating solution was applied to the cleaned silicone substrates, which were fixed on the custom holder at the center of the spin coater device, rotating at 3000 rpm for 30 s. After the coating process, all the films were dried at 70°C for 10 minutes to evaporate the solvent and binder from the films. As for laser film processing, the prepared graphene films underwent a processing step using a pulsed Nd:YAG laser. With an energy of 300 mJ, a repetition rate of 6 Hz, a wavelength of 1064 nm, and a number of different pulses of 50 and 150, with a circular spot with a large diameter of about 3 mm. The spot was kept large to contain irradiated areas suitable for physical measurements.

3. Results and Discussion

In Fig. (1a), the x-ray diffraction (XRD) patterns of graphene films prepared by spin coating and deposited on n-type silicon showed a peak of high intensity at a diffraction angle of 69° and a direction of (100). In addition to another peak located almost at an angle of 26.5°, which corresponds the (002) crystallographic direction of graphene according to (JCPDS card 96-120-0019). Where (002) is the preferred growth direction for graphene, this trend is consistent in graphene and carbon structure of the hexagonal lattice. There is no change in dominant orientation with increasing number of pulses. As for the graphene samples deposited on the surface of p-type silicon, there is no significant difference compared to the samples deposited on n-type silicon, as it is also noted that a peak of high intensity appears at an angle of 69°, which belongs to silicon with a direction of (100), as shown in Fig. (1b).

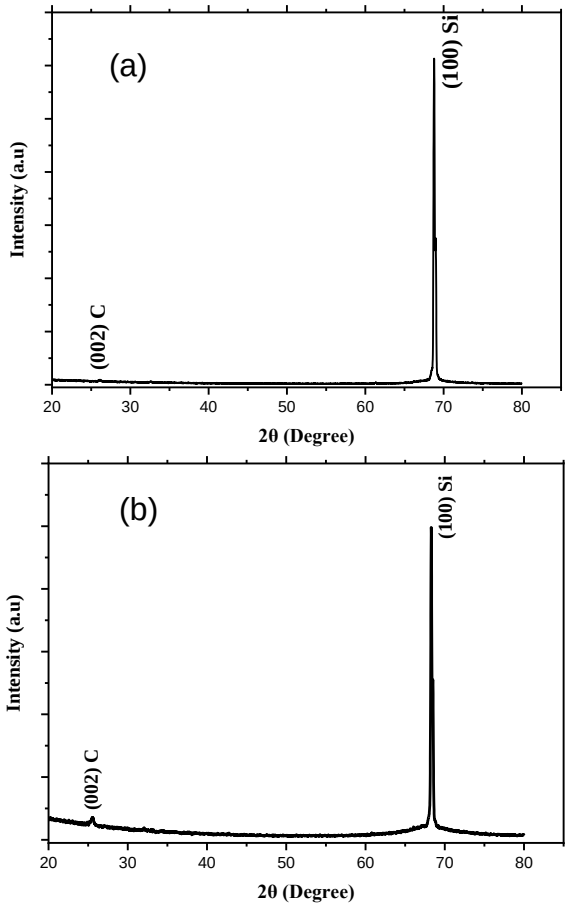

Fig. (1) XRD patterns of prepared thin films (a) graphene films deposited on n-type silicon. (b) graphene films deposited on p-type silicon

The FWHM of graphene peak was determined using Origin software and compared with the accompanying results of the XRD data sheet. It can be seen that the peak width increases after laser treatment, and the increase continues with the increase in the number of pulses, and this indicates a decrease in crystalline size. A slight shift is observed at the peak from one sample to another due to the appearance or decrease of stress in the lattice due to an increase or decrease in crystalline size. Stress was calculated using the following equation [21]:

$$\varepsilon = \frac{\beta \cos\theta}{4} \quad (1)$$

In addition, the crystallite size (D) was calculated and the values of d-spacing and micro strain were given with x-ray examination. As shown in tables (1) and (2). Crystallite size was also calculated based on peak exposure using Debye-Scherrer equation [21]:

$$D = \frac{0.9\,\lambda}{\beta\,\cos\theta} \qquad (2)$$

where λ the wavelength (1.54Å), and β represents FWHM of diffraction peak

The distances between crystallographic planes (d_{hkl}) were also calculated using the diffraction angle 2θ according to Bragg's law. It is noted from the two tables that the crystallite size of the (002) direction, which represents the thickness of the graphene layer, lies within the nanoscale for all samples and the crystal size decreases when the number of laser pulses increases. On the other hand, we notice an increase in lattice stresses with a decrease in crystal size as a result of the inverse relationship between them [22,23]. This change in structural properties has an impact on other physical properties, as these properties can be controlled by controlling the number of laser pulses used to process the films.

When graphene is treated with 50 and 150 laser pulses, it should be noted that graphene peak intensity begins to decrease as the number of pulses increases due to the reduction of graphene layer on the Si substrate. It is also noted that graphene peak changes slightly as a result of the decrease in crystallite size and the change in the lattice strain values in both cases (*n* and *p*) and as shown in Fig. (2).

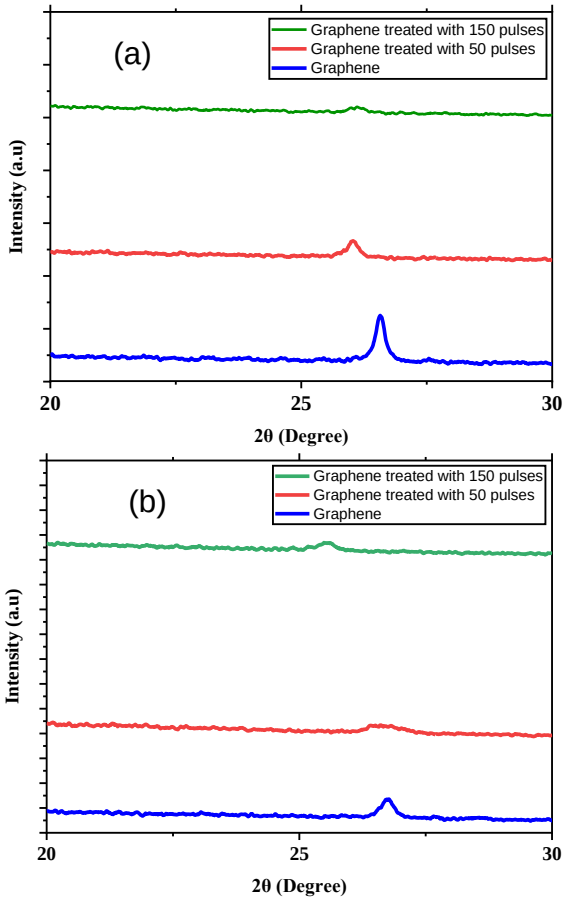

Fig. (2) Diffraction peaks of graphene in (0-50-150) pulsed laser (a) graphene deposited on n-type silicon, (b) graphene deposited on p-type silicon

The morphology of graphene films deposited on n-type and p-type silicon substrates before and after laser treatment was analyzed using field-emission scanning electron microscopy (FE-SEM). Figure (3) shows FE-SEM images of graphene films deposited on n-type and p-type silicon substrates with different number of laser pulses. Number of laser pulses may result in multiple effects in the laser processing and the interaction with matter. Increasing the number of laser pulses results in more chemically active interactions between the material and the laser, affecting the material's structure and surface.

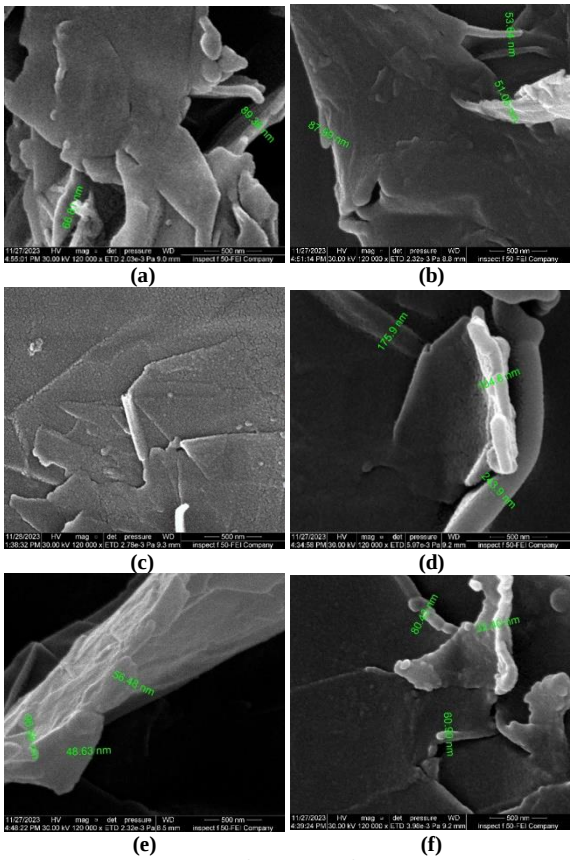

Fig. (3) FE-SEM images of graphene films deposited on (a) n-type and before laser treatment. (b) 50 pulses. (c) 150 pulses. (d) p-type before laser treatment. (e) 50 pulses. (f) 150 pulses

Figures (3a,b,c) show FE-SEM images of graphene samples deposited on n-type silicon substrates. At 0, 50, and 150 laser pulses, the samples appear in the form of cohesive wrinkled flakes with a crystal size ranging between 89-36 nm, respectively. As the number of pulses increases, a mixture of a smooth flakes appears. Using 150 pulses, smooth and complete graphene layers evenly distributed on the surface are clearly formed. There is a noticeable difference in the surface morphology of laser-treated samples, especially in samples prepared using 150 pulses, where they appear broader and smoother, forming wavy surfaces. As for the samples deposited on a p-type silicon substrate shown in figures (3d,e,f), the effect of laser treatment appears clearly through a change in the nature of the surface, a reduction in the

number of layers, a decrease in the crystalline size of the samples with an increase in the number of pulses, in addition to a change in the shape of the surface from scattered flakes to a more uniform and smooth surface. Also, the nanoscale range for all samples decreases with the increase in the number of pulses used to enhance the thin film. There is also a noticeable decrease in the number of graphene layers for samples deposited on p-type silicon with an increase in the number of pulses from 50 to 150 pulses. On the other hand, lattice strains decrease with increasing number of pulses due to their inverse relationship with a particle size. The difference in the structure or surface morphology of the deposited material composition. They contribute to evaporation and exchange of particles from the sample surface. This can lead to the formation of different structures based on interactions and exchanges between atoms and molecules. Increasing the number of pulses can affect the surface temperature rise, melting and ambient chemical reactions, which contribute to structure changes and increased crystallinity of the deposited material and lead to rapid removal of oxygen and water in graphene resulting in the breakage of graphene sheets in the original material. Additional heating due to increased pulsation.

Energy-dispersive x-ray spectroscopy (EDX) is used to identify the elements involved in the composition of prepared films and analyzes the atomic and weight ratios of these elements. Table (3) shows the atomic and weight ratios of the chemical elements involved in preparing samples for graphene films deposited on n-type and p-type silicon substrates before and after pulsed laser treatment. Also, it shows a clear decrease in the intensity of the carbon peak with an increase in the number of laser pulses due to peeling (reduction) of the material from the surface, as this leads to a decrease in the film thickness with an increase in the number of pulses. Therefore, the carbon peak decreased and the silicon peak increased, in addition to the difference in oxygen percentages in the samples due to the temperature generated by the incident energy of repeated laser pulses, which leads to the consumption of oxygen or its oxidation when it interacts with the air.

Figures (4) and (5) show 3D images of the surface topography of graphene films prepared and deposited on n-type and p-type silicon substrates, respectively, before and after laser treatment. It was found that the AFM results are affected by the type of substrate, shape, behavior and surface nature of the nanoparticles and the nanoparticle solution used. It was also observed that the surface of the samples was affected by the laser energy and the number of pulses, which led to the surface peeling and homogeneity as a result of engraving when the number of pulses increased. The appearance of grains and pits was also observed on the p-type substrate. As for the n-type substrate, we notice a clear roughness on the surface. Also, the size of the component composing the composite decreases and the surface becomes more homogeneous when the films are irradiated with a pulsed laser. It was noted that the number of graphene layers decreased after laser irradiation, as shown in the table (4).

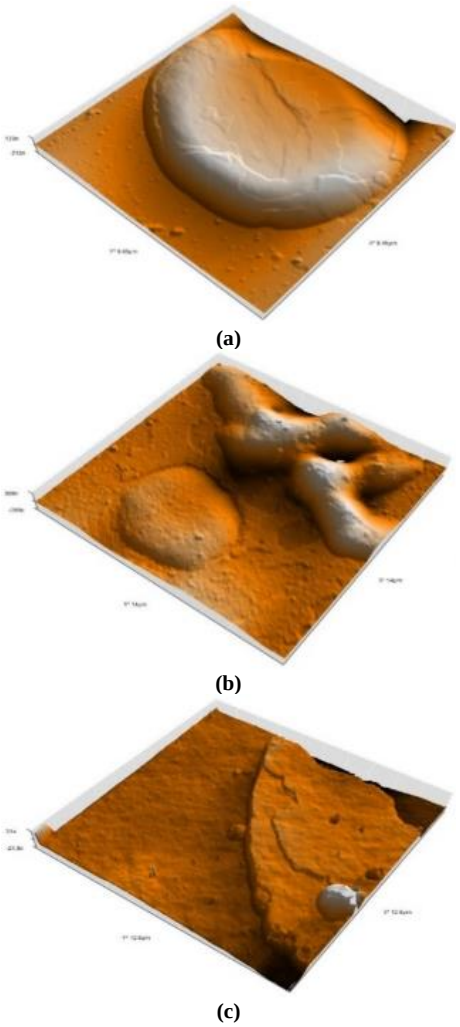

(a) **(b)** **(c)**

Fig. (4) 3D AFM images of graphene deposited on n-type silicon (a) graphene before laser treatment, (b) with 50 pulses, (c) with 150 pulses

Table (4) Thickness of graphene films deposited on n-type and p-type silicon substrates before and after laser treatment

Substrate type	Number of pulses	Thickness (nm)
n-type	0	41.43
	50	8.583
	150	3.340
p-type	0	119.3
	50	39.22
	150	13.32

Figure (6) shows Fourier-transform infrared (FTIR) spectra within the wavenumber range of 400-4000 cm^{-1} for graphene films deposited on n-type and p-type silicon substrates, respectively. Before and after pulsed laser treatment. The spectrum consists of vibrational groups from graphene layer including carbonyl (C=O), aromatic (C=C), carboxyl (COOH), epoxy (CO-C) and hydroxyl (O-H) groups [24,25],

whereas the sharp peak at 3441 cm^{-1} corresponds to (O-H) which belongs to the (C-OH) carboxyl groups with the possible presence of water molecules due to humidity, and the absorption peaks at 2937 cm^{-1} and 2837 cm^{-1} represent the asymmetric and symmetric vibrations of the CH_2 bonds. As for the peaks that appeared at 1728.22 and 1705.07 cm^{-1} in the n-type laser-treated samples, and at 1695.43 cm^{-1} for the sample before treatment, they are due to the ketone group (C=O), and the main graphite field at 1581.63, 1475.54, 1552.70, and 1517.98 cm^{-1} is due to sp^2 hybridization and is related to the vibrations of the aromatic ring of graphene. The (O-H) deformation occurs at 1411.89 cm^{-1}, and 1271.19, 1271.09, and 1296.16 cm^{-1} indicate the (C-O) expansion of the epoxy groups, and 1082.07, 1016.49, and 1037.70 cm^{-1} stretching (C-O) for the alkoxy groups, and 912.33, 923.90, and 929.69 cm^{-1} refers to the epoxy or peroxide group, and the absorption peaks (694-472 cm^{-1}) refer to bending vibrations (C-H).

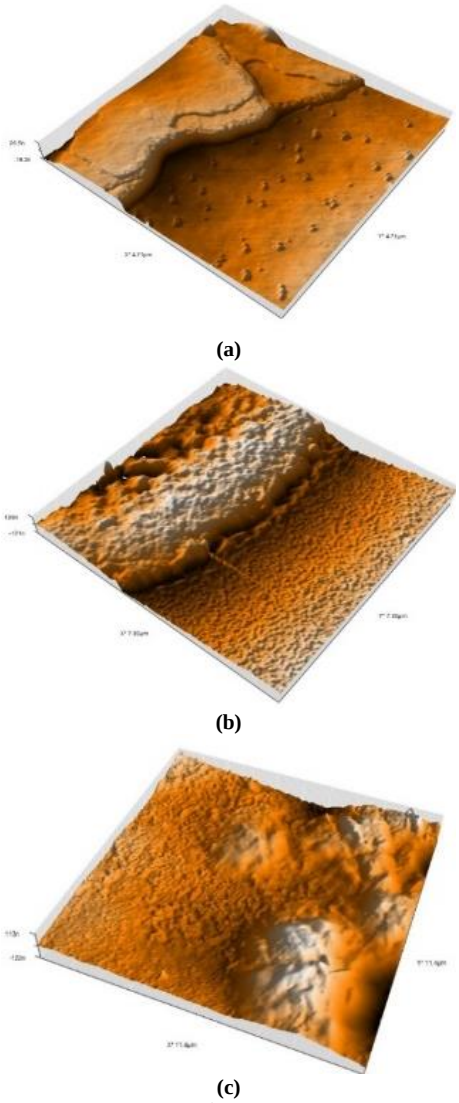

(a)

(b)

(c)

Fig. (5) AFM-3D images of graphene deposited on p-type silicon (a) graphene before laser treatment, (b) 50 pulses, (c) 150 pulses

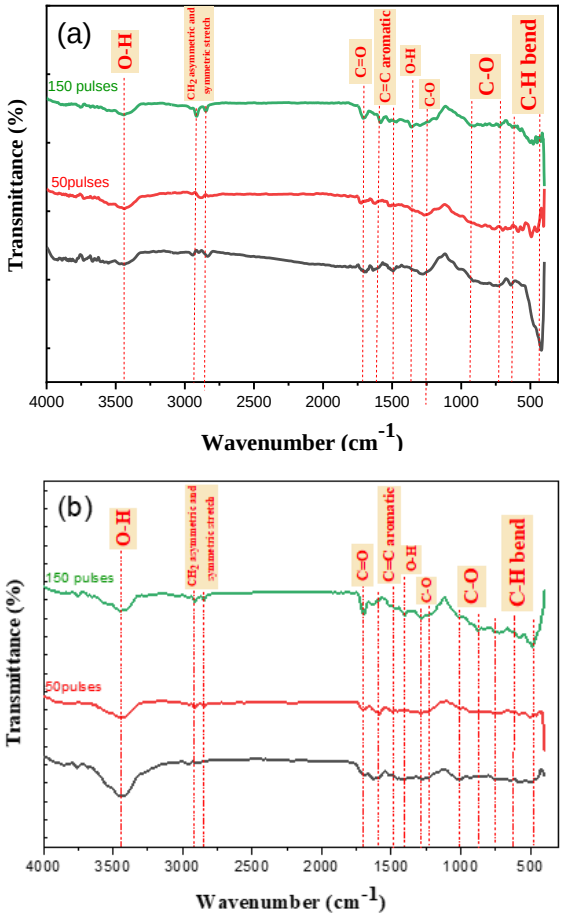

Fig. (6) FTIR spectra of graphene samples deposited on (a) n-type silicon and (b) p-type silicon s. before and after laser treatment

As for graphene samples deposited on p-type silicon, the peaks at 1703-1701 cm^{-1} are due to the ketone group (C=O), and the peaks at 1622, 1693, and 1637 cm^{-1} and 1460, 1585, and 1523 cm^{-1} are all due to vibrations in the aromatic ring of graphene, and a peak appears at 1404 cm^{-1} due to bending or deformation (O-H), and 1375 and 1367 cm^{-1} indicate stretching (C-O) of the carboxy groups, and 1240, 1234, and 1273 cm^{-1} due to the (C-O) expansion of the epoxy groups, and 1002, 1008, and 1016 cm^{-1} due to the (C-O) expansion of the alkoxy groups, and 931 and 933 cm^{-1} return to the epoxy or peroxide group, and the absorption peaks are at 754, and 717 cm^{-1}, 584, 574, and 592 cm^{-1}, and 489, 493, and 480 cm^{-1}, all of which are also due to (C-H) bending vibrations.

A clear change can be observed in the n-type FTIR spectra due to the strengthening of the (π) bond in graphene (carbon atoms) by reducing defects, which ultimately leads to closing the conduction gap and enhancing electrical conductivity of n-type, in contrast to the p-type, which does not show a significant change [26,27].

Photoluminescence (PL) spectroscopy was used to calculate the energy band gap value of the prepared graphene films according to the energy gap equation, which is [28]:

$$E_g = \frac{1240}{\lambda} \quad (3)$$

where λ represents the highest peak of wavelength

As shown in Fig. (7), there are two prominent peaks the high peak within the wavelength range of 520-560 nm belonged to graphene, they are attributed to the recombination of electron-hole pairs in local state of sp^2 carbon cluster embedded in sp^3 matrix, while the second peak which is slightly smaller in the range 260-280 nm belonged to silicon substrates.

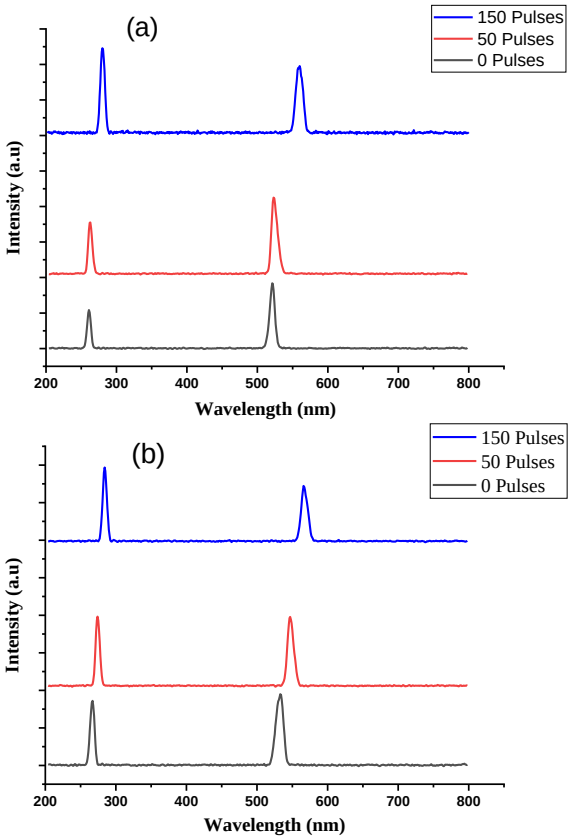

Fig. (7) PL spectra of graphene films deposited on (a) n-type silicon substrates, (b) on p-type silicon substrates, before and after laser treatment

Table (5) Peaks of PL spectra and energy gap values of graphene samples deposited on n-type and p-type silicon substrates

Substrate type	Number of pulses	Wavelength (nm)	E_g (eV)
n-type	0	521.94	2.376
	50	524.02	2.366
	100	532.05	2.33
	150	560	2.20
p-type	0	533.97	2.32
	50	545.97	2.27
	100	556.02	2.23
	150	567.05	2.19

Table (5) shows the energy gap values. The band gap of graphene varies depending on the oxygen groups present in the structure. The PL density of graphene increases to 560 at 150 pulses for the n-type and 567 for the p-type. The peak shows a shift towards red wavelengths with increasing number of pulses. The decrease in the oxygen-bound group may allow energy gap values to be controlled using the type of substrate and determining the pulse energy and number upon laser treatment applied, which is consistent with references [29-31].

4. Conclusion

Using pulsed laser treatment technology is an ideal way to peel layers of graphene without using any chemicals or high temperatures over long periods of time. Peeling of multilayer graphene layers has been achieved using this technique. It was also observed that the graphene thickness and crystal size decreased significantly when the number of laser pulses was increased. This method has proven its efficiency in reducing graphene layers in an easy, fast and energy-efficient method. The surface morphological properties of graphene were also improved after increasing the number of pulses to some extent to avoid coalition or breakage of the layers as a result of the high temperature. One of the advantages of this technology is improving chemical bonds and obtaining strengthening areas that increase the interconnection of graphene molecules and layers. In addition, reducing graphene layers increases its conductivity and makes it more attractive for use in micro-devices such as sensors, detectors, and many optoelectronic devices.

References

[1] L.A. Kolahalam et al., "Review on nanomaterials: Synthesis and applications", in *Materials Today: Proc.*, Elsevier Ltd (2019), pp. 2182–2190.

[2] S. Singh et al., "Graphene nanomaterials: The wondering material from synthesis to applications", *Sens. Int.*, 3 (2022) 100190.

[3] W. Nakanishi et al., "Bioactive nanocarbon assemblies: Nanoarchitectonics and applications", *Nano Today*, 9(3) (2014) 378–394.

[4] A.L. Olatomiwa et al., "Recent advances in density functional theory approach for optoelectronics properties of graphene", *Heliyon*, 9(3) (2023) e14279.

[5] A. Beltaos et al., "Damage effects on multi-layer graphene from femtosecond laser interaction", *Physica Scripta*, Topical Issues (2014) 014015.

[6] C. Backes et al., "Production and processing of graphene and related materials", *2D Mater*, 7(2) (2020) 022011.

[7] Y. Xiao et al., "Synthesis and Functionalization of Graphene Materials for Biomedical Applications: Recent Advances, Challenges, and Perspectives", *Adv. Sci.*, 10(9) (2023) 05292.

[8] G. Li et al., "Graphene Fabrication by Using Femtosecond Pulsed Laser and Its Application on Passively Q-Switched Solid-State Laser as Saturable Absorber", *IEEE Photon. J.*, 12(2) (2020) 2966217.

[9] R. Trusovas et al., "Graphene layer formation in pinewood by nanosecond and picosecond laser irradiation", *Appl. Surf. Sci.*, 471 (2018) 154-161.
[10] S.F.S. Al-Tikrity and R. Vickers, "Measuring the optical transmittance of graphene with silicon substrates within a particular range of the spectrum from the terahertz to infrared regime", in *Int. Conf. on Infrared, Millimeter, and Terahertz Waves, IRMMW-THZ* (2014).
[11] Y. Zhao et al., "Integrated graphene systems by laser irradiation for advanced devices", *Nano Today*, 12 (2017) 14-30.
[12] E.E. Ghadim et al., "Pulsed laser irradiation for environment friendly reduction of graphene oxide suspensions", *Appl. Surf. Sci.*, 301 (2014) 183-188.
[13] M. Makarov, A. Timoshkov and A. Borisov, "Terahertz Lasing Using Optically Excited Neutral Donor Centres Embedded in Crystalline Silicon", *Iraqi J. Mater.*, 3(3) (2024) 17-24.
[14] R. Kumar et al., "Laser-assisted synthesis, reduction and micro-patterning of graphene: Recent progress and applications", *Coordin. Chem. Rev.*, 342 (2017) 34–79.
[15] K.T. Paula et al., "Laser patterning and induced reduction of graphene oxide functionalized silk fibroin", *Opt. Mater.*, 99 (2020) 109540.
[16] A. Vasquez et al., "Micro-structuring, ablation, and defect generation in graphene with femtosecond pulses", *OSA Contin.*, 2(10) (2019) 2925.
[17] Y. Zhou et al., "Microstructuring of graphene oxide nanosheets using direct laser writing", *Adv. Mater.*, 22(1) (2010) 67-71.
[18] S. Papazoglou et al., "Direct laser printing of graphene oxide for resistive chemosensors", *Opt. Laser Technol.*, 82 (2016) 163–169.
[19] O.A. Hammadi, "Characteristics of Thermally-Annealed Homojunction Silicon Photodetector Prepared by Low-Pressure Plasma-Assisted Technique", *Iraqi J. Appl. Phys. Lett.*, 7(2) (2024) 3-6.
[20] R.J. Mohammed, J.M. Mansoor and A.A. Kamil, "A Detailed Evaluation of Zn:Cu Co-Doping Impacts on the Performance of Nanostructured CdO Thin Films", *Iraqi J. Appl. Phys.*, 20(3) (20240 469-476.
[21] A.K. Singh, **"Advanced X-ray Techniques in Research and Industries"**, IOS Press (Amsterdam, 2005), p. 126, 251.
[22] B.M. Ghdhaib and S.N. Rashid, "Characterization of Nickel and Nickel Oxide Nanoparticles Prepared by Laser Ablation Technique: Effect of Laser Wavelength and Energy." *Iraqi J. Appl. Phys.*, 20(3) (2024) 477-484.
[23] S.W. Chan and W. Wang, "Surface stress of nano-crystals", *Mater. Chem. Phys.*, 273 (2021) 125091.
[24] L. Silipigni, L. Torrisi and M. Cutroneo, "Physical investigations on the radiation damage of graphene oxide by IR pulsed laser", in *EPJ Web of Conferences*, EDP Sciences, Jan. 2018. Doi: 10.1051/epjconf/201816705011.
[25] M. Cutroneo et al., "Localized modification of graphene oxide properties by laser irradiation in vacuum", *Vacuum*, 165 (2019) 134–138.
[26] M.M. Jasim and S.F.S. Al-Tikrity, "Depositing Layers of Nano Graphene on p-Type Silicon Substrate and Studying the Structural and Optical Properties", *J. Res. Appl. Sci. Biotech.*, 2(5) (2023) 83–88.
[27] M. Bera et al., "Facile One-Pot Synthesis of Graphene Oxide by Sonication Assisted Mechanochemical Approach and Its Surface Chemistry", *J. Nanosci. Nanotechnol.*, 18(2) (2017) 902–912.
[28] J.H. Dellinger, **"Calculation of Planck's Constant"**, National Bureau of Standards (NBS) Bulleting, 7 (1911) 393.
[29] K. Murawski et al., "HgCdTe Energy Gap Determination from Photoluminescence and Spectral Response Measurements", *Metrol. Measur. Syst.*, 30(1) (2023) 183–194.
[30] G. Witjaksono et al., "Effect of nitrogen doping on the optical bandgap and electrical conductivity of nitrogen-doped reduced graphene oxide", *Molecules*, 26(21) (2021) 26216424.
[31] M.V. Narayana and S.N. Jammalamadaka, "Tuning Optical Properties of Graphene Oxide under Compressive Strain Using Wet Ball Milling Method", *Graphene*, 5(2) (2016) 73-80.

Table (1) Structural parameters of graphene thin films deposited on n-type silicon

Laser pulses	2θ (Deg.)	FWHM (Deg.)	d-spacing (Å)	Crystallite Size (D) (nm)	Micro Strain (ε)	hkl
None	26.5523	0.1826	3.35431	78.09	0.43037	(002)
50	26.0904	1.1492	3.42059	62.43	0.50972	(002)
150	26.0794	1.1845	3.34606	62.37	0.56091	(002)

Table (2) Structural parameters of graphene thin films deposited on p-type silicon

Laser pulses	2θ (Deg.)	FWHM (Deg.)	d-spacing (Å)	Crystallite Size (D) (nm)	Micro Strain (ε)	hkl
None	26.7098	0.4141	3.33488	98.44	1.1425	(002)
50	26.6388	0.7535	3.34361	73.64	1.4677	(002)
150	25.4616	0.7538	3.49547	63.52	1.64991	(002)

Table (3) EDX data of graphene samples deposited on n-type and p-type silicon substrates before and after laser treatment

	n-type			p-type		
	Element	Atomic %	Weight %	Element	Atomic %	Weight %
	Before laser treatment					
	C	64.2	43.7	C	60.0	39.3
	O	0.9	0.8	O	0.9	0.8
	Si	34.9	55.5	Si	39.1	60.0
	After laser treatment					
50 pulses	C	63.4	42.9	C	59.7	38.9
	O	0.9	0.8	O	0.6	0.6
	Si	35.6	56.3	Si	39.7	60.6
150 pulses	C	51.3	31.3	C	54.2	33.4
	O	1.2	1.0	O	0.7	0.6
	Si	47.5	67.8	Si	45.1	66

